Research Square

Preprints are preliminary reports that have not undergone peer review.
They should not be considered conclusive, used to inform clinical practice,
or referenced by the media as validated information.

A novel de novo DNM1L mutation linked to mitochondrial fission dysfunction in a pediatric patient with epileptic encephalopathy and refractory seizures

M. Javier Herrero-Turrión

mjaviht@usal.es

Universidad de Salamanca (USAL)

Aranzazu Hernández-Fabian

Universidad de Salamanca (USAL)

Ricardo Gómez-Nieto

Universidad de Salamanca (USAL)

Julia Sánchez-Sánchez

Universidad de Salamanca (USAL)

María José López-Martínez

CIEN Foundation, Alzheimer's Centre Queen Sofía Foundation

Alberto Rábano-Gutiérrez

CIEN Foundation, Alzheimer's Centre Queen Sofía Foundation

Pablo Prieto-Matos

Universidad de Salamanca (USAL)

María Isidoro-García

Universidad de Salamanca (USAL)

Research Article

Keywords: DNM1L, DRP1, encephalopathy, epilepsy, EMPF1

Posted Date: July 20th, 2026

DOI: https://doi.org/10.21203/rs.3.rs-10199543/v1

License: This work is licensed under a Creative Commons Attribution 4.0 International License.
Read Full License

Additional Declarations: No competing interests reported.

Version of Record: A version of this preprint was published at Orphanet Journal of Rare Diseases on September 30th, 2026. See the published version at https://doi.org/10.1186/s13023-026-04636-4.

Abstract

Background

Mitochondrial dynamics are essential for neuronal function, with dynamin-related protein 1 (DRP1), encoded by the *DNM1L* gene, playing a key role in mitochondrial fission. Pathogenic variants in *DNM1L* are associated with a spectrum of severe neurodevelopmental and neurodegenerative disorders. This study aimed to characterize the clinical, genetic, and pathological features of a novel *DNM1L* variant and to elucidate its impact on DRP1 function and mitochondrial physiology.

Results

A case study was performed by integrating clinical phenotyping, metabolic and neuroimaging evaluation, whole-exome sequencing, in silico modeling, postmortem histopathology, and functional analyses using western blotting and neuronal assays to assess DRP1 expression and mitochondrial morphology. The patient, a 12-year-old female, presented with developmental delay, microcephaly, ataxia, refractory seizures, and behavioral disturbances. Brain MRI was unremarkable, but metabolic testing revealed elevated lactate levels and abnormal EEG patterns. Whole-exome sequencing identified a novel heterozygous de novo *DNM1L* variant (c.1093A > G; p.Arg365Gly) located in the DRP1 middle domain and classified as likely pathogenic. *In silico* modeling predicted disruption of stabilizing intramolecular interactions and altered protein packing. Postmortem neuropathology revealed widespread neurodegeneration, neuronal loss, and gliosis. Functional assays demonstrated decreased levels of monomeric and oligomeric DRP1 and pronounced mitochondrial hyperfusion, consistent with defective mitochondrial fission due to impaired DRP1 oligomerization.

Conclusions

This work identifies and functionally characterizes a novel *DNM1L* variant, broadening the clinical and genetic spectrum of DRP1-associated mitochondrial disorders. The findings underscore the importance of integrated clinical, genetic, structural, and functional analyses to elucidate the mechanistic basis of rare mitochondrial diseases.

Introduction

Mitochondrial fission and fusion are highly dynamic processes that are essential for maintaining mitochondrial homeostasis within the nervous system and other tissues. Disruptions in the proteins regulating these processes can impair mitochondrial dynamics, leading to abnormal fission and fusion, which are associated with a range of clinical disorders [1].

In humans, Dynamin-Related Protein 1 (DRP1) is an 81.8 kDa protein that plays a critical role in mitochondrial and peroxisomal fission. It is encoded by the *dynamin 1-like* (*DNM1L*) gene, located on chromosome 12p11.21 (21 exons), and shares high homology with other dynamin family proteins. DRP1 contains an N-terminal GTPase domain (GD), responsible for generating the mechanical force required for membrane constriction, a middle domain (MD) that mediates DRP1 oligomerization, and a C-terminal GTPase effector domain (GED), which enhances GTPase activity and stabilizes the DRP1 homodimer complex. In addition, DRP1 harbors a non-conserved variable domain (VD) that modulates protein function [2–5].

DRP1 is a cytosolic protein that forms homodimers and is recruited to the outer mitochondrial membrane and peroxisomal surface, where it mediates fission. This process occurs through a GTP hydrolysis–dependent mechanism in which DRP1 wraps around the scission site, constricts, and ultimately severs the membrane [6]. Excessive activation or upregulation of *DNM1L* is linked to aberrant mitochondrial fragmentation, contributing to neuronal damage in distinct neurodegenerative disorders [7]. Moreover, studies in a neural cell–specific *Drp1-/-* mouse model highlight the crucial role of DRP1 in embryonic forebrain and cerebellar development, as well as synapse formation [8–9].

Pathogenic variants in *DNM1L* underlie two neurological disorders (Online Mendelian Inheritance in Man; MIM*603850): Encephalopathy, lethal, due to defective Mitochondrial and Peroxisomal Fission 1 (EMPF1, MIM #614388) and Optic atrophy 5 (OPA5, MIM #610708). EMPF1, caused by either monoallelic or biallelic *DNM1L* variants, is commonly associated with developmental delay, hypotonia, refractory epilepsy, and premature death [10]. To date, at least 79 affected individuals with 40 distinct pathogenic variants have been reported: 21 cases with 16 variants in the GD of DRP1, 51 cases with 18 variants in the MD, 1 case with a variant in the VD, and 6 cases with five variants in the GED (Table 1) [3, 10–56].

Here, we report a pediatric patient carrying a novel heterozygous *DNM1L* variant, c.1093A > G (p.Arg365Gly), located in the MD of DRP1. The patient presented profound developmental delays and severe neurological impairment. To our knowledge, this variant has not been previously described. We provide a detailed characterization of the clinical features and the associated cellular phenotype.

Material and methods

Participants and samples

The patient, family members, and three unrelated pediatric controls were recruited under informed written consent, as approved by the Institutional Review Boards of the University Hospital of Salamanca and the Neurological Tissue Bank at the Institute of Neuroscience of Castilla y León (BTN-INCYL). Tissue samples, including frozen brain sections, were provided by BTN-INCYL and analyzed anonymously. Sample transfer was conducted in accordance with national regulations governing research on human biological materials. Postmortem tissue handling and preparation followed the standard BTN-INCYL

protocol. Neuropathological autopsy was performed within 10 hours of death, initiated upon notification by the donor's proxies. The right hemisphere of the brain was sectioned and frozen at − 80°C, while the left hemisphere was fixed in 4% phosphate-buffered formaldehyde for at least three weeks.

Whole-exome sequencing

Genomic DNA was extracted from peripheral blood using a magnetic bead–based method on a MagnaPure Instrument (Roche Diagnostics, Switzerland). Libraries were prepared using TruSeq (Illumina, San Diego, CA) and xGen Exome technology (Integrated DNA Technologies, Coralville, IA). Sequencing was performed on a NextSeq500 platform (Illumina). Bioinformatic analysis was carried out using the GRCh37/hg19 reference genome.

In-silico protein 3D structure analysis and modeling

An *in-silico* workflow adapted from Díaz-Rodríguez et al. [57] was applied to evaluate the structural and functional consequences of the *DNM1L* c.1093A > G variant. Protein structure prediction for wild-type and p.Arg365Gly mutant DRP1 was performed using AlphaFold2, which predicts amino acid distance distributions via deep learning and generates 3D atomic coordinates. Molecular graphics, including mesh and helix/loop representations, were rendered with PyMOL (Version 1.8, Schrödinger, LLC). Dynamic visualization was generated from VRML files using Cortona Movie Maker (Parallel Graphics, Boston, MA) at 1024 × 768 resolution. Interatomic interactions were assessed with Arpeggio. Solvent Accessible Surface Area (SASA) was measured with PyMOL, and ΔSASA values ($\Delta SASA = SASA_{Mutant} - SASA_{WT}$) were calculated to evaluate changes in solvent exposure. Residue-level ΔSASA values were plotted in Microsoft Excel.

To evaluate the thermodynamic impact of the mutation on protein stability, five *in silico* prediction tools were employed, including DynaMut2, INPS3D, FoldX5.1, MAESTRO, and PremPS [57–59]. These tools estimate changes in Gibbs free energy (ΔΔG), with destabilizing mutations defined as $\Delta\Delta G < 0$ for DynaMut2 and INPS3D, and $\Delta\Delta G > 0$ for FoldX5.1, MAESTRO, and PremPS. DynaMut2 integrates molecular dynamics and normal mode analysis to evaluate stability changes with atomic-level precision, while INPS3D incorporates sequence-based features, physicochemical properties, and structural determinants such as solvent accessibility and local energy variations [57–58]. FoldX5.1 applies an empirical force field to assess the effects of mutations on protein folding, stability, and interactions, whereas MAESTRO employs statistical scoring functions and machine learning-based ensemble predictions to determine stability alterations [57]. PremPS, which relies on ten evolutionary and structural features, is trained on a balanced dataset of stabilizing and destabilizing mutations, enhancing predictive accuracy, particularly for stabilizing variants [59].

Histology, immunohistochemistry and image analysis

Fixed brain tissue was routinely processed, paraffin-embedded, and sectioned at 6 µm. Sections were deparaffinized, rehydrated through graded alcohols, and stained with hematoxylin and eosin (H&E) following standard protocols to assess cytoarchitecture and cellular morphology. Brightfield images were captured on a Leica DMRB microscope (Leica Biosystems) fitted with a DP50 digital camera (Olympus) using 4×, 10× and 20× objectives for low magnification and 40× or 100× oil objectives for higher magnification. Morphometric measurements and cell-dot mapping were carried out with the open-source software ImageJ (version 1.53c; NHI, USA). Additionally, DRP1 and the mitochondrial marker TOMM20 were evaluated by immunofluorescence in the cerebellum and prefrontal cortex using confocal microscopy. To accomplish this, deparaffinized tissue sections were subjected to heat-induced epitope retrieval using 10 mM citrate buffer (pH 6.0) at ≥ 100°C for 15 min. Sections were blocked in 5% normal goat serum, 2% bovine serum albumin and 0.25% Triton X-100 and incubated overnight at 4°C with primary antibodies: rabbit anti-DNM1L (DRP1; PA1-16987, Invitrogen) at 1:500 and rabbit anti-TOMM20 (MA5-32148, Invitrogen) at 1:200. After washes, sections were incubated with Alexa Fluor–conjugated secondary antibodies (anti-rabbit Alexa Fluor 555, 1:500), nuclei counterstained with DAPI, and nonspecific autofluorescence quenched using 0.3% Sudan Black. Confocal image acquisition was performed on a Leica Stellaris 8 confocal microscope using a 63×/NA 1.4 oil objective. Z-stacks were collected with optical sectioning appropriate to the objective (≈ 0.3 µm steps), and three-dimensional projections were generated by maximum intensity and stereo z-projection. Negative control sections processed without primary antibody showed no specific signal. All photomicrographs used in the figures underwent only minor and uniform adjustments to brightness and contrast, along with removal of tissue-free background in Adobe Photoshop® CS3 (Version 10.0) and were subsequently assembled in Canvas 14.

Western blot analysis

Protein extracts from cerebellum and prefrontal cortex were prepared in lysis buffer (10 mM Tris, pH 7.4; 150 mM NaCl; 2 mM EDTA; 1% NP-40; protease and phosphatase inhibitors). Lysates were clarified by centrifugation, denatured in Laemmli buffer, and subjected to SDS-PAGE. Proteins were probed with rabbit anti-DNM1L (1:500, Invitrogen, #PA1-16987) and rabbit anti-βIII-tubulin (1:6000, Sigma, #T2200). Secondary antibody detection was performed with peroxidase-conjugated goat anti-rabbit IgG (1:8000, Jackson ImmunoResearch, #111-035-003). Signals were imaged using a MicroChemi 4.2 Chemiluminescence System.

Statistical analysis

Statistical analyses, including quantification of western blot band intensities, were performed with SPSS v20 (IBM, Chicago, IL, USA). Group comparisons were assessed by ANOVA (Fisher's post hoc test) and Student's t-test. Results with $p < 0.05$ were considered statistically significant (*). Quantitative data are presented as mean ± standard deviation (SD) and were plotted using GraphPad Prism v8.

Results

Case presentation and clinical manifestation

The patient was a 12-year-old female, second child of non-consanguineous Caucasian parents, born at 38 weeks from a twin pregnancy complicated by fetal growth restriction. The family pedigree is shown in Fig. 1A. At birth, she presented low weight (1,570 g) and length (40 cm) and was treated with growth hormone. From infancy, she exhibited severe global developmental delay, microcephaly, and encephalopathy. Motor development was markedly delayed, with independent walking at 3 years and persistent ataxia with pyramidal signs. Speech was significantly impaired, with limited vocabulary acquisition. Behavioral disturbances included hyperactivity, impulsiveness, and aggression, along with episodes of motor regression. At 9 years, she developed refractory status epilepticus triggered by influenza A, followed by recurrent convulsive and non-convulsive episodes, often infection related. Her condition progressed to dysphagia and chronic respiratory failure requiring non-invasive ventilation. No dystonia, neuropathy, or sensory deficits were observed, and cardiological and ophthalmological evaluations were normal. She died at 12 years.

Metabolic studies showed transient lactate elevation (< 3.3 mmol/L) during seizures, with otherwise normal biochemical profiles. Brain Magnetic Resonance Imaging (MRI) at 3 and 10 years was unremarkable. Serial electroencephalograms (EEGs) revealed generalized slowing without interictal epileptiform activity, while seizures showed multifocal patterns, including right parieto-occipital and left frontotemporal involvement.

Conventional karyotyping revealed no abnormalities, while chromosomal microarray analysis (array-CGH) identified a ~ 730 kb interstitial gain at 18q22.1b of uncertain significance. Whole-exome sequencing identified a heterozygous *DNM1L* c.1093A > G variant (NM_012062.4) in exon 10, resulting in a p.Arg365Gly substitution (NP_036192.2) within the MD of DRP1. The variant was confirmed by Sanger sequencing. Segregation analysis showed that both parents and the healthy sibling carried the wild-type allele, confirming a *de novo* origin (Fig. 1A). This variant has not been previously reported and was classified as likely pathogenic according to ACMG/ACGS guidelines [60]. It has been submitted to the Leiden Open Variation Database (ID #00466853). The affected residue (Arg365) is highly conserved across species, and no other pathogenic variants explaining the phenotype were identified.

Structural impact of the p.Arg365Gly variant in DNM1L

To investigate the molecular consequences of the missense variant in exon 10 of the human *DNM1L* gene (c.1093A > G; p.Arg365Gly), we generated a predicted 3D model of the encoded protein. This substitution replaces arginine with glycine at position 365 within the MD, potentially affecting DRP1 structure and function (Fig. 1B-F and Supplementary Material 1). Structural analysis using AlphaFold2 models of wild-type and mutant DRP1 revealed local conformational changes in the MD (Fig. 1B). In the wild type, Arg365 is surface-exposed, whereas Gly365 in the mutant becomes more buried (Fig. 1C). This substitution removes a bulky, positively charged residue, allowing surrounding residues to shift inward

and tighten local packing. Although both residues remain within the same α-helix, the mutation alters the local structural environment (Fig. 1B-C). Detailed interaction analysis showed a marked loss of stabilizing contacts in the mutant protein, including reductions in van der Waals interactions, hydrogen bonds, and polar interactions, along with complete loss of hydrophobic and ionic interactions (Fig. 1D; Supplementary Material 1). These changes indicate disruption of the native interaction network. SASA analysis demonstrated an 11% decrease in exposure at residue 365 (Fig. 1E), with compensatory increases in nearby residues (+ 11% -Tyr368-, 7% -Glu359-; Fig. 1E), suggesting localized structural rearrangements. Energetic predictions using multiple stability algorithms (DynaMut2, INPS3D, FoldX, MAESTRO, and PremPS) consistently indicated a destabilizing effect of the mutation, with ΔΔG values ranging from − 1.69 to + 1.06 kcal/mol (Fig. 1F; Supplementary Material 1).

Neuropathological findings in the postmortem brain

Macroscopic examination revealed a markedly atrophic brain weighing 670 g (< 50% of the expected weight for age), without focal lesions or malformations. There was diffuse cortical atrophy with moderate ventricular dilation (Fig. 2). Microscopically, cortical regions showed disruption of normal laminar architecture, with extensive neuronal loss, gliosis, and neuropil rarefaction (Figs. 3 and 4). These changes were most prominent in deeper layers (V–VI), particularly in frontal, insular, and occipital cortices, and in some areas extended through the full cortical thickness (Fig. 3A–B). The neuropil displayed a microvacuolated (spongiform) appearance, with numerous small, clear spaces reflecting tissue rarefaction. Neurons appeared shrunken with eosinophilic, achromatic cytoplasm, consistent with advanced degeneration, alongside mild gliosis (Fig. 3a1–B). In addition to the cortical involvement, the juxtacortical white matter exhibited prominent gliosis, vascular proliferation, and moderate spongiform change (Fig. 3c1). The hippocampus showed distorted cytoarchitecture and marked vacuolization, indicating severe parenchymal disorganization (Fig. 4A, 4a1). Subcortical regions, including the nucleus basalis of Meynert, demonstrated neurons with granular, achromatic cytoplasm, suggestive of metabolic or degenerative changes. The hypothalamus and thalamus showed moderate to severe gliosis with significant neuronal loss and reactive changes (Fig. 4B, 4b1). In the brainstem, gliosis and neuronal loss were observed in the midbrain, substantia nigra, and oculomotor nuclei, with similar changes in pontine and medullary motor nuclei. Some neurons exhibited cytoplasmic microvacuolation, consistent with early degeneration (data not shown). The cerebellum largely preserved its laminar organization, with most Purkinje cells appearing morphologically normal (Fig. 4C, 4c1). However, occasional Purkinje cells showed microvacuolation, and axonal spheroids were present, indicating focal degeneration (Fig. 4c2). Finally, gliosis was also noted in the dentate nucleus without significant neuronal loss (data not shown).

DRP1 protein levels and immunohistopathological findings

To evaluate the effect of the *DNM1L* variant (c.1093A > G; p.Arg365Gly) on DRP1 protein levels, Western blot analysis was performed on lysates from the prefrontal cortex and cerebellum, compared with pediatric controls (Fig. 5). Two bands (~ 75 kDa and ~ 280 kDa) corresponding to monomeric and

oligomeric DRP1 were detected. Mutant samples showed a marked reduction in both forms, particularly the oligomeric fraction.

Immunohistochemistry further assessed mitochondrial morphology. Cerebellar neurons harboring the mutation exhibited pronounced mitochondrial hyperfusion, with enlarged, balloon-like structures absent in controls (Fig. 6). These neurons also showed increased DRP1 immunostaining (Fig. 6). In contrast, staining for the mitochondrial marker TOMM20 was significantly reduced compared to controls (Fig. 7). Similar alterations were observed in prefrontal cortex neurons (data not shown).

Discussion

Mitochondria are highly dynamic organelles that continuously undergo fission, fusion, and migration. The genes encoding mitochondrial dynamics–related proteins are nuclear, and variants in these genes can lead to mitochondrial diseases and neurodegenerative disorders such as Parkinson's disease, Alzheimer's disease, and amyotrophic lateral sclerosis [1, 7]. Alterations in the *DNM1L* gene, which encodes DRP1, have been associated with *de novo* dominant-negative mutations that cause early-onset encephalopathy and lethality due to defective mitochondrial and peroxisomal fission. To date, at least 79 EMPF1 patients have been reported, harboring at least 40 distinct *DNM1L* variants (Table 1). All cases exhibit neurocognitive dysfunction attributable to mitochondrial impairment, though the spectrum and severity of symptoms vary widely. Clinical phenotypes range from severe neonatal hypotonia leading to early death to developmental delay or regression with or without epilepsy. In general, pathogenic variants affecting the DRP1 MD appear to be more severe than those involving the GD or GED domain. For example, psychomotor retardation and epilepsy were less common in patients with GD variants compared with those carrying MD variants [10, 42]. As summarized in Table 1, at least 18 pathogenic MD variants have been reported in 51 patients [12–19, 21, 25–27, 31–32, 34–35, 37–41, 43–44, 47–51, 53–54, 56]. These variants are thought to impair oligomerization, disrupt GTPase-dependent conformational contraction, and ultimately compromise mitochondrial fission [4]. Most are *de novo* mutations and are associated with a high incidence of developmental delay/regression and epilepsy. Furthermore, in a large proportion of these patients, biochemical, neuroimaging, and electrophysiological studies revealed elevated lactate levels, abnormal brain MRI findings, and abnormal EEG [10].

In this study, we describe a novel heterozygous *DNM1L* variant, c.1093A > G (p.Arg365Gly), in a 12-year-old female patient. This variant, located in the DRP1 MD and predicted to be likely pathogenic according to ACGS/ACMG guidelines, was associated with significant developmental delay and neurological impairment. Notably, the most distinguishing clinical feature of this case is the presence of ataxia with no brain MRI abnormalities. In summary, the patient presented with developmental delay, microcephaly, encephalopathy, ataxia, behavioral problems (hyperactivity, impulsivity, and aggression), generalized tonic–clonic seizures, and refractory status epilepticus. No dystonia, peripheral neuropathy, pain insensitivity, dysarthria, strabismus, or MRI abnormalities were observed.

Compared with the lethal *DNM1L* variants p.Ala395Asp and p.Cys431Tyr [13, 51, 53], the phenotype in our case resembles that described by Vanstone et al. [48] with a Gly362Asp mutation, where the patient showed prolonged survival, nonspecific refractory epilepsy, and fewer clinical manifestations. Another case involving a different substitution at the same DRP1 position (p.Gly362Ser) was also characterized by postnatal microcephaly and developmental delay [43]. However, that patient exhibited pain insensitivity, likely due to sensory neuropathy [43], which was not observed in our case. Whitley et al. [53] described a patient with a milder phenotype associated with a missense variant at position Ala395 compatible with survival (p.Ala395Gly), as well as another patient with the recurrent p.Arg403Cys variant, reported in nine additional cases [12, 15–16, 21, 26, 32, 34–35, 37, 40–41, 49–50, 53–54].The phenotypic differences between p.Ala395Asp and p.Ala395Gly, as well as between p.Gly362Asp and p.Gly362Ser, highlight the functional sensitivity of this region of DRP1 while underscoring that the ultimate effect depends on the specific physicochemical properties of the substitution.

Our *in silico* structural analysis provides a mechanistic explanation for the pathogenicity of the p.Arg365Gly variant. Using AlphaFold2-generated 3D models, we observed that although both Arg365 and Gly365 lie within the same α-helical segment, the substitution induces substantial changes in local residue environment and surface topology. Arg365, solvent-exposed in the wild-type configuration, becomes significantly buried when replaced by glycine, a finding quantitatively supported by a ΔSASA of − 11%. This is consistent with the physicochemical contrast between arginine, which forms extensive stabilizing interactions via its guanidinium group, and glycine, which lacks a side chain and thus reduces steric and interaction potential. The substitution permits inward shifting of neighboring residues, compacting the local structure and effectively burying Gly365 deeper within the protein. Compensatory increases in solvent exposure for Tyr368 and Glu359 further suggest local rearrangement consistent with core-packing defects [61].

Structural modeling also revealed a loss of key intermolecular contacts at the mutation site. The p.Arg365Gly substitution led to a marked reduction in van der Waals forces, hydrogen bonds, and polar interactions, as well as a complete loss of hydrophobic contacts, ionic bonds, and cation–π interactions. This collapse of the local interaction network underscores the critical role of Arg365 in stabilizing the MD. Importantly, all five computational stability predictors used in this study (DynaMut2, INPS3D, FoldX, MAESTRO, and PremPS) independently classified the p.Arg365Gly mutation as destabilizing. Notably, this consensus was observed despite differences in their underlying algorithms and ΔΔG interpretation thresholds. The convergence of these predictions reinforces the conclusion that the mutation compromises the thermodynamic stability of DRP1. This aligns with previous benchmarking studies, which have demonstrated that such agreement among diverse prediction tools reflects their overall reliability in identifying destabilizing mutations [62].

Such destabilization is likely to impact higher-order DRP1 assembly. DRP1 co-assembles with mitochondrial receptor MID49 to form helical oligomers essential for mitochondrial membrane scission [63]. The MD, where Arg365 resides, is central for both self-assembly and receptor interactions [mitochondrial fission factor (MFF) and mitochondrial dynamics proteins (MID49 and MID51] [64].

Recruitment of DRP1 to mitochondria and subsequent GTP hydrolysis trigger conformational changes necessary for oligomerization and membrane fission [1, 6]. Thus, disruption of the MD, as seen with p.Arg365Gly, likely impairs oligomerization and compromises fission activity.

Postmortem brain analysis of our patient revealed moderate ventricular dilation and widespread neurodegenerative changes affecting multiple cortical (frontal, insular, occipital, entorhinal, and perirhinal) and subcortical (hypothalamus, thalamus, midbrain, and cerebellum) regions, characterized by marked neuronal loss and gliosis. Similar findings have been reported in patients with the p.Arg403Cys variant [32, 40]. Additional pathological changes observed in our patient, such as cytoplasmic achromasia, granular patterns, and neuronal microvacuolation, are consistent with neuronal degeneration described in other *DNM1L*-related cases [37].

Biochemical analysis confirmed decreased DRP1 expression in cerebellar and prefrontal cortex extracts, affecting two distinct bands of approximately 75 kDa and 280 kDa in our samples, corresponding to the monomeric and oligomeric forms of DRP1, respectively [3]. These oligomers represent homotetramers, consistent with the mechanism of DRP1 association with the mitochondrial membrane [6]. This mirrors findings in fibroblasts from patients with other pathogenic *DNM1L* variants, including p.Thr59Asn and p.Arg710Gly [28, 38], as well as compound heterozygous cases [36]. Conversely, some variants such as p.Gly401Ser and p.Arg403Cys have been associated with normal DRP1 levels, while p.Phe370Cys was linked to increased levels [30, 38, 49]. Taken together, our data suggest that p.Arg365Gly disrupts oligomerization, consistent with the effects of neighboring variants Gly363Asp and Gly401Ser [38] and other stalk domain mutations, including lethal p.Ala395Asp and p.Gly350Arg [13].

We further observed profound mitochondrial hyperfusion in patient neurons, with giant balloon-like organelles resembling nucleoid aggregation, a phenotype previously linked to DRP1 downregulation [65]. Impaired mitochondrial fission produces hyperfused networks, as shown in neurons of the basal ganglia of *Dnm1l* knockout mice [8–9,70] and in multiple pathogenic variants (p.Gly32Ala, p.Asp146Asn, p.Gly363Asp, p.Ala395Asp, p.Gly401Ser, p.Arg403Cys, p.Cys431Tyr, p.Arg710Gly) and a GTPase-deficient recombinant mutant (p.Lys38Ala) [13, 30, 38, 51, 53]. Importantly, Longo et al. [17] demonstrated that mitochondrial hyperfusion in p.Asp146Asn fibroblasts impairs mitostasis by slowing degradation due to steric hindrance of enlarged mitochondria, not defective autophagy. Interestingly, while p.Asp146Asn fibroblasts did not show increased mitochondrial mass; our patient with p.Arg365Gly displayed reduced TOMM20 immunoreactivity, consistent with impaired mitochondrial distribution, similar to variants p.Gly223Val, p.Phe370Cys, and p.Arg403Cys [49]. These findings support a dominant-negative mechanism, in which impaired oligomerization causes widespread hyperfusion and defective mitochondrial fission.

Conclusion

This study shows a novel de novo heterozygous *DNM1L* variant, p.Arg365Gly, in a Spanish patient with clinical features overlapping those of previously reported cases. Our findings expand the spectrum of

DNM1L-related disorders and emphasize their heterogeneity. Genetic testing remains essential for diagnosis, given the broad phenotypic variability. This study provides new insights into the structural and functional consequences of MD variants in DRP1 and contributes to a deeper understanding of their role in mitochondrial pathology, with potential implications for clinical diagnosis and management.

Abbreviations

DNM1L
Dynamin 1-like
DRP1
Dynamin-Related Protein 1
EMPF1
Encephalopathy Mitochondrial and Peroxisomal Fission 1
GD
N-terminal GTPase domain
GED
C-terminal GTPase effector domain
H&E
Hematoxylin and eosin
MD
Middle domain
MRI
Brain Magnetic Resonance Imaging
SASA
Solvent Accessible Surface Area

Declarations

Acknowledgements

We express our sincere gratitude to the patient and his family for their invaluable participation, without which this work would not have been possible. The authors also thank Dr. Olga Serrano Ayestarán for her essential role in facilitating the patient's donation and Carlos García-Peral for his expert guidance regarding 3D protein structure analysis and the use of stability predictors.

Author contributions

MJHT, AHF, PPM, RGN, and MIG contributed significantly to the conception, design, acquisition, analysis, and interpretation of data. AHF, PPM, and MIG performed patient follow-up and genetic diagnosis. AR and MJLM performed pathological analysis. RGM performed analysis of protein 3D structures and stability predictors. JSS performed experiments and protein expression analysis. All authors contributed to the article and approved the submitted version.

Funding

This work was supported by the Instituto de Investigación Biomédica de Salamanca (IBSAL) through the contributions given to the Banco de Tejidos Neurológicos del Instituto de Neurociencias de Castilla y León (BTN-INCYL), Instituto de Neurociencias de Castilla y León (INCYL), University of Salamanca. This study has also been funded by Instituto de Salud Carlos III (ISCIII) through the project "PI25/01904" and co-financed with European Union (PIs: Ricardo Gómez-Nieto).

Data availability

All data generated or analyzed during this study are included in this published article.

Ethical Approval

The studies involving humans were approved by the Medical Ethics Committee of University Hospital of Salamanca (2023-11). The studies were conducted in accordance with local legislation and institutional requirements. Written informed consent for participation and publication was obtained from the patient's legal guardian(s). Written informed consent was obtained from the individual(s), and minor(s)' legal guardian/next of kin, for the publication of any potentially identifiable images or data included in this article. No details that might disclose the identity of the subjects under study have been included.

Consent for publication

Informed consent was obtained from the parents of all individual participants included in the study.

Competing interests

The authors have no competing interests to declare. The authors did not receive funding from any organization for preparation of the submitted work.

Author details

[1] Banco de Tejidos Neurológicos del Instituto de Neurociencias de Castilla y León (BTN-INCYL), Salamanca, Spain; [2] Instituto de Neurociencias de Castilla y León (INCyL), Salamanca, Spain; [3] Instituto de Investigación Biomédica de Salamanca (IBSAL), Salamanca, Spain; [4] Universidad de Salamanca (USAL), Salamanca, Spain; [5] Dpto. de Biología Celular y Patología, USAL, Salamanca, Spain; [6] Dpto. de Ciencias Biomédicas y del Diagnósticas, USAL, Salamanca, Spain; [7] Neuropathology and Biobank Platform, CIEN Foundation, Alzheimer's Centre Queen Sofía Foundation, Madrid, Spain; [8] Unidad de Referencia Regional de Diagnóstico Avanzado de Enfermedades Raras de Castilla y León (DiERCyL), Salamanca, Spain; [9] Dpto. de Pediatría, Hospital Universitario de Salamanca, Salamanca, Spain; [10] Dpto. Medicina, USAL, Salamanca, Spain; [11] Dpto. de Bioquímica Clínica, Hospital Universitario de Salamanca, Salamanca, Spain, Salamanca, Spain

References

1. Al Ojaimi M, Salah A, El-Hattab AW. Mitochondrial fission and fusion: molecular mechanisms, biological functions, and related disorders. Membranes. 2022;12:9. http://doi:10.3390/membranes12090911.
2. Schrader M, Bonekamp NA, Islinger M. Fission and proliferation of peroxisomes. Biochim Biophys Acta. 2012;1822:1343–57.
3. Hogarth KA, Costford SR, Yoon G, Sondheimer N, Maynes JT. *DNM1L* variant alters baseline mitochondrial function and response to stress in a patient with severe neurological dysfunction. Biochem Genet. 2018;56:56–77.
4. Tilokani L, Nagashima S, Paupe V, Prudent J. Mitochondrial dynamics: overview of molecular mechanisms. Essays Biochem. 2018;62:341–60.
5. Assia Batzir N, Bhagwat PK, Eble TN, Liu P, Eng CM, Elsea SH, Robak LA, Scaglia F, Goldman AM, Dhar SU, Wangler MF. De novo missense variant in the GTPase effector domain (GED) of *DNM1L* leads to static encephalopathy and seizures. Cold Spring Harb Mol Case Stud. 2019;5:a003673.
6. Koirala S, Guo Q, Kalia R, Bui HT, Eckert DM, Frost A, Shaw JM. Interchangeable adaptors regulate mitochondrial dynamin assembly for membrane scission. Proc Natl Acad Sci U S A. 2013;110:E1342–51.
7. Joshi AU, Minhas PS, Liddelow SA, Haileselassie B, Andreasson KI, Dorn GW 2. Mochly-Rosen D. Fragmented mitochondria released from microglia trigger A1 astrocytic response and propagate inflammatory neurodegeneration. Nat Neurosci. 2019;22:1635–48.
8. Ishihara N, Nomura M, Jofuku A, Kato H, Suzuki SO, Masuda K, Otera H, Nakanishi Y, Nonaka I, Goto Y, Taguchi N, Morinaga H, Maeda M, Takayanagi R, Yokota S, Mihara K. Mitochondrial fission factor Drp1 is essential for embryonic development and synapse formation in mice. Nat Cell Biol. 2009;11:958–66.
9. Wakabayashi J, Zhang Z, Wakabayashi N, Tamura Y, Fukaya M, Kensler TW, Iijima M, Sesaki H. The dynamin-related GTPase Drp1 is required for embryonic and brain development in mice. J Cell Biol. 2009;186:805–16.
10. Zhang Z, Bie X, Chen Z, Liu J, Xie Z, Li X, Xiao M, Zhang Q, Zhang Y, Yang Y, Li D. A novel variant of *DNM1L* expanding the clinical phenotypic spectrum: a case report and literature review. BMC Pediatr. 2024;24:104.
11. Berti B, Verrigni D, Nasca A, Di Nottia M, Leone D, Torraco A, Rizza T, Bellacchio E, Legati A, Palermo C, Marchet S, Lamperti C, Novelli A, Mercuri EM, Bertini ES, Pane M, Ghezzi D, Carrozzo R. De novo *DNM1L* mutation in a patient with encephalopathy, cardiomyopathy and fatal non-epileptic paroxysmal refractory vomiting. Int J Mol Sci. 2024;25:7782.
12. Brunet T, Jech R, Brugger M, Kovacs R, Alhaddad B, Leszinski G, Riedhammer KM, Westphal DS, Mahle I, Mayerhanser K, Skorvanek M, Weber S, Graf E, Berutti R, Necpál J, Havránková P, Pavelekova P, Hempel M, Kotzaeridou U, Hoffmann GF, Leiz S, Makowski C, Roser T, Schroeder SA, Steinfeld R,

Strobl-Wildemann G, Hoefele J, Borggraefe I, Distelmaier F, Strom TM, Winkelmann J, Meitinger T, Zech M, Wagner M. De novo variants in neurodevelopmental disorders—experiences from a tertiary care center. Clin Genet. 2021;100:14–28.

13. Chang CR, Manlandro CM, Arnoult D, Stadler J, Posey AE, Hill RB, Blackstone C. A lethal de novo mutation in the middle domain of the dynamin-related GTPase Drp1 impairs higher order assembly and mitochondrial division. J Biol Chem. 2010;285:32494–503.
14. Chao YH, Robak LA, Xia F, Koenig MK, Adesina A, Bacino CA, Scaglia F, Bellen HJ, Wangler MF. Missense variants in the middle domain of *DNM1L* in cases of infantile encephalopathy alter peroxisomes and mitochondria when assayed in Drosophila. Hum Mol Genet. 2016;25:1846–56.
15. Chen X, Li Y, Luo H, Gan J. Analysis of *DNM1L* gene variant in a case of fatal encephalopathy caused by mitochondrial peroxidase division deficiency. Chin J Med Genet. 2021;38:887–90.
16. De Souza Crippa AC, Franklin GL, Takeshita BT, Ghizoni Teive HA. *DNM1L* mutation presenting as progressive myoclonic epilepsy associated with acute febrile infection-related epilepsy syndrome. Epileptic Disord. 2022;24:976–78.
17. Delanne J, Bruel AL, Huet F, Moutton S, Nambot S, Grisval M, Houcinat N, Kuentz P, Sorlin A, Callier P, Jean-Marcais N, Mosca-Boidron AL, Mau-Them FT, Denommé-Pichon AS, Vitobello A, Lehalle D, El Chehadeh S, Francannet C, Lebrun M, Lambert L, Jacquemont ML, Gerard-Blanluet M, Alessandri JL, Willems M, Thevenon J, Chouchane M, Darmency V, Fatus-Fauconnier C, Gay S, Bournez M, Masurel A, Leguy V, Duffourd Y, Philippe C, Feillet F, Faivre L, Thauvin-Robinet C. The diagnostic rate of inherited metabolic disorders by exome sequencing in a cohort of 547 individuals with developmental disorders. Mol Genet Metab Rep. 2021;29:100812.
18. Díez H, Cortès-Saladelafont E, Ormazábal A, Marmiese AF, Armstrong J, Matalonga L, Bravo M, Briones P, Emperador S, Montoya J, Artuch R, Giros M, Garcia-Cazorla À. Severe infantile parkinsonism because of a de novo mutation on DLP1 mitochondrial-peroxisomal protein. Mov Disord. 2017;32:1108–10.
19. Dong X, Liu B, Yang L, Wang H, Wu B, Liu R, Chen H, Chen X, Yu S, Chen B, Wang S, Xu X, Zhou W, Lu Y. Clinical exome sequencing as the first-tier test for diagnosing developmental disorders covering both CNV and SNV: a Chinese cohort. J Med Genet. 2020;57:558–66.
20. Dzinovic I, Boesch S, Škorvánek M, Necpál J, Švantnerová J, Pavelekova P, Havránková P, Tsoma E, Indelicato E, Runkel E, Held V, Weise D, Janzarik W, Eckenweiler M, Berweck S, Mall V, Haslinger B, Jech R, Winkelmann J, Zech M. Genetic overlap between dystonia and other neurologic disorders: a study of 1100 exomes. Parkinsonism Relat Disord. 2022;102:1–6.
21. Fahrner JA, Liu R, Perry MS, Klein J, Chan DC. A novel de novo dominant negative mutation in *DNM1L* impairs mitochondrial fission and presents as childhood epileptic encephalopathy. Am J Med Genet A. 2016;170:2002–11.
22. Hiraide T, Yamoto K, Masunaga Y, Asahina M, Endoh Y, Ohkubo Y, Matsubayashi T, Tsurui S, Yamada H, Yanagi K, Nakashima M, Hirano K, Sugimura H, Fukuda T, Ogata T, Saitsu H. Genetic and

phenotypic analysis of 101 patients with developmental delay or intellectual disability using whole-exome sequencing. Clin Genet. 2021;100:40–50.

23. Kahrizi K, Hu H, Hosseini M, Kalscheuer VM, Fattahi Z, Beheshtian M, Suckow V, Mohseni M, Lipkowitz B, Mehvari S, Mehrjoo Z, Akhtarkhavari T, Ghaderi Z, Rahimi M, Arzhangi S, Jamali P, Falahat Chian M, Nikuei P, Sabbagh Kermani F, Sadeghinia F, Jazayeri R, Tonekaboni SH, Khoshaeen A, Habibi H, Pourfatemi F, Mojahedi F, Khodaie-Ardakani MR, Najafipour R, Wienker TF, Najmabadi H, Ropers HH. Effect of inbreeding on intellectual disability revisited by trio sequencing. Clin Genet. 2019;95:151–9.
24. Keller N, Paketci C, Edem P, Thiele H, Yis U, Wirth B, Karakaya M. De novo *DNM1L* variant presenting with severe muscular atrophy, dystonia and sensory neuropathy. Eur J Med Genet. 2021;64:104134.
25. Kim SH, Kim B, Lee JS, Kim HD, Choi JR, Lee ST, Kim HD, Choi JR, Lee ST, Kang HC. Proband-only clinical exome sequencing for neurodevelopmental disabilities. Pediatr Neurol. 2019;99:47–54.
26. Ladds E, Whitney A, Dombi E, Hofer M, Anand G, Harrison V, Fratter C, Carver J, Barbosa IA, Simpson M, Jayawant S, Poulton J. De novo *DNM1L* mutation associated with mitochondrial epilepsy syndrome with fever sensitivity. Neurol Genet. 2018;4:e258.
27. Lecoquierre F, Duffourd Y, Vitobello A, Bruel AL, Urteaga B, Coubes C, Garret P, Nambot S, Chevarin M, Jouan T, Moutton S, Orphanomix Physician's Group, Tran-Mau-Them F, Philippe C, Sorlin A, Faivre L, Thauvin-Robinet C. Variant recurrence in neurodevelopmental disorders: the use of publicly available genomic data identifies clinically relevant pathogenic missense variants. Genet Med. 2019;21:2504–11.
28. Lhuissier C, Wagner BE, Vincent A, Garraux G, Hougrand O, Van Coster R, Benoit V, Karadurmus D, Lenaers G, Gueguen N, Chevrollier A, Maystadt I. Case report: thirty-year progression of an EMPF1 encephalopathy due to defective mitochondrial and peroxisomal fission caused by a novel de novo heterozygous *DNM1L* variant. Front Neurol. 2022;13:937885.
29. Liu X, Zhang Z, Li D, Lei M, Li Q, Liu X, Zhang P. *DNM1L*-related mitochondrial fission defects presenting as encephalopathy: a case report and literature review. Front Pediatr. 2021;9:626657.
30. Longo F, Benedetti S, Zambon AA, Sora MGN, Di Resta C, De Ritis D, Quattrini A, Maltecca F, Ferrari M, Previtali SC. Impaired turnover of hyperfused mitochondria in severe axonal neuropathy due to a novel DRP1 mutation. Hum Mol Genet. 2020;29:177–88.
31. Magistrati M, Zupin L, Lamantea E, Baruffini E, Ghezzi D, Legati A, Celsi F, Murru FM, Capaci V, Pinamonti M, Bussani R, Carrozzi M, Dallabona C, Zeviani M, Bonati MT. De novo *DNM1L* pathogenic variant associated with lethal encephalocardiomyopathy—case report and literature review. Int J Mol Sci. 2025;26:846.
32. Mancardi MM, Nesti C, Febbo F, Cordani R, Siri L, Nobili L, Lampugnani E, Giacomini T, Granata T, Marucci G, Consales A, Rossi A, Luria G, Santorelli FM, Buratti S. Focal status and acute encephalopathy in a 13-year-old boy with de novo *DNM1L* mutation. Brain Dev. 2021;43:644–51.
33. Marouane A, Neveling K, Deden AC, van den Heuvel S, Zafeiropoulou D, Castelein S, van de Veerdonk F, Koolen DA, Simons A, Rodenburg R, Westra D, Mensenkamp AR, de Leeuw N, Ligtenberg M,

Matthijsse R, Pfundt R, Kamsteeg EJ, Brunner HG, Gilissen C, Feenstra I, de Boode WP, Yntema HG, van Zelst-Stams WAG, Nelen M, Vissers LELM. Lessons learned from rapid exome sequencing for 575 critically ill patients. Front Genet. 2023;14:1304520.

34. McCormack M, McGinty R, Zhu X, Slattery L, Heinzen EL, Costello EPIGENC, Delanty DJ, Cavalleri N. De novo mutations in patients with chronic ultra-refractory epilepsy. Eur J Med Genet. 2020;63:103625.
35. Minghetti S, Giorda R, Mastrangelo M, Tassi L, Zanotta N, Galbiati S, Bassi MT, Zucca C. Epilepsia partialis continua associated with the p.Arg403Cys variant of the *DNM1L* gene. Epileptic Disord. 2022;24:176–82.
36. Nasca A, Legati A, Baruffini E, Nolli C, Moroni I, Ardissone A, Goffrini P, Ghezzi D. Biallelic mutations in *DNM1L* are associated with a slowly progressive infantile encephalopathy. Hum Mutat. 2016;37:898–903.
37. Nolan DA, Chen B, Michon AM, Salatka E, Arndt D. Expanding the *DNM1L*-associated intractable epilepsy and encephalopathy phenotype. Epileptic Disord. 2019;21:112–6. http://doi:10.1684/epd.2019.1046.
38. Nolden KA, Egner JM, Collier JJ, Russell OM, Alston CL, Harwig MC, Widlansky ME, Sasorith S, Barbosa IA, Douglas AG, Baptista J, Walker M, Donnelly DE, Morris AA, Tan HJ, Kurian MA, Gorman K, Mordekar S, Deshpande C, Samanta R, McFarland R, Hill RB, Taylor RW, Oláhová M. Novel *DNM1L* variants impair mitochondrial dynamics. Life Sci Alliance. 2022;5:e202101284.
39. Piccoli C, Scrima R, D'Aprile A, Chetta M, Cela O, Pacelli C, Ripoli M, D'Andrea G, Margaglione M, Bukvic N, Capitanio N. Pathogenic *DNM1L* variant linked to infantile progressive neurological disorder. Genes (Basel). 2021;12:1295.
40. Ryan CS, Fine AL, Cohen AL, Schiltz BM, Renaud DL, Wirrell EC, Patterson MC, Boczek NJ, Liu R, Babovic-Vuksanovic D, Chan DC, Payne ET. De novo *DNM1L* variant in a teenager with progressive paroxysmal dystonia. J Child Neurol. 2018;33:651–8.
41. Schmid SJ, Wagner M, Goetz C, Makowski C, Freisinger P, Berweck S, Mall V, Burdach S, Juenger H. A de novo dominant negative mutation in *DNM1L* causes sudden onset status epilepticus. Neuropediatrics. 2019;50:197–201.
42. Schon KR, Horvath R, Wei W, Calabrese C, Tucci A, Ibañez K, Ratnaike T, Pitceathly RDS, Bugiardini E, Quinlivan R, Hanna MG, Clement E, Ashton E, Sayer JA, Brennan P, Josifova D, Izatt L, Fratter C, Nesbitt V, Barrett T, McMullen DJ, Smith A, Deshpande C, Smithson SF, Festenstein R, Canham N, Caulfield M, Houlden H, Rahman S, Chinnery PF, Genomics England Research Consortium. Use of whole genome sequencing to determine genetic basis of suspected mitochondrial disorders. BMJ. 2021;375:e066288.
43. Sheffer R, Douiev L, Edvardson S, Shaag A, Tamimi K, Soiferman D, Meiner V, Saada A. Postnatal microcephaly and pain insensitivity due to a de novo heterozygous *DNM1L* mutation. Am J Med Genet A. 2016;170:1603–7.

44. Tarailo-Graovac M, Zahir FR, Zivkovic I, Moksa M, Selby K, Sinha S, Nislow C, Stockler-Ipsiroglu SG, Sheffer R, Saada-Reisch A, Friedman JM, van Karnebeek CDM, Horvath GA. De novo pathogenic *DNM1L* variant in atypical hereditary sensory and autonomic neuropathy. Mol Genet Genomic Med. 2019;7:e00961.
45. Trujillano D, Bertoli-Avella AM, Kumar Kandaswamy K, Weiss ME, Köster J, Marais A, Paknia O, Schröder R, Garcia-Aznar JM, Werber M, Brandau O, Calvo Del Castillo M, Baldi C, Wessel K, Kishore S, Nahavandi N, Eyaid W, Al Rifai MT, Al-Rumayyan A, Al-Twaijri W, Alothaim A, Alhashem A, Al-Sannaa N, Al-Balwi M, Alfadhel M, Rolfs A, Abou Jamra R. Clinical exome sequencing: results from 2819 samples. Eur J Hum Genet. 2017;25:176–82.
46. Van der Ven AT, Johannsen J, Kortüm F, Wagner M, Tsiakas K, Bierhals T, Lessel D, Herget T, Kloth K, Lisfeld J, Scholz T, Obi N, Wortmann S, Prokisch H, Kubisch C, Denecke J, Santer R, Hempel M. Prevalence and clinical prediction of mitochondrial disorders. Clin Genet. 2021;100:766–70.
47. Vandeleur D, Chen CV, Huang EJ, Connolly AJ, Sanchez H, Moon-Grady AJ. Novel and lethal case of cardiac involvement in *DNM1L* mitochondrial encephalopathy. Am J Med Genet A. 2019;179:2486–9.
48. Vanstone JR, Smith AM, McBride S, Naas T, Holcik M, Antoun G, Harper ME, Michaud J, Sell E, Chakraborty P, Tetreault M, Care4Rare Consortium, Majewski J, Baird S, Boycott KM, Dyment DA, MacKenzie A, Lines MA. *DNM1L*-related mitochondrial fission defect presenting as refractory epilepsy. Eur J Hum Genet. 2016;24:1084–8.
49. Verrigni D, Di Nottia M, Ardissone A, Baruffini E, Nasca A, Legati A, Bellacchio E, Fagiolari G, Martinelli D, Fusco L, Battaglia D, Trani G, Versienti G, Marchet S, Torraco A, Rizza T, Verardo M, D'Amico A, Diodato D, Moroni I, Lamperti C, Petrini S, Moggio M, Goffrini P, Ghezzi D, Carrozzo R, Bertini E. Clinical-genetic features and peculiar muscle histopathology in infantile *DNM1L*-related mitochondrial epileptic encephalopathy. Hum Mutat. 2019;40:601–18.
50. Wang AS, Lemire G, van Noy GE, Austin-Tse C, O'Donnell-Luria A, Kilbane C. *DNM1L* variant presenting as adolescent-onset sensory neuronopathy. J Pediatr Neurol. 2023;21:475–8.
51. Waterham HR, Koster J, van Roermund CW, Mooyer PA, Wanders RJ, Leonard JV. A lethal defect of mitochondrial and peroxisomal fission. N Engl J Med. 2007;356:1736–41.
52. Wei Y, Qian M. Case report: a novel de novo mutation in *DNM1L* presenting with developmental delay, ataxia, and peripheral neuropathy. Front Pediatr. 2021;9:604105.
53. Whitley BN, Lam C, Cui H, Haude K, Bai R, Escobar L, Hamilton A, Brady L, Tarnopolsky MA, Dengle L, Picker J, Lincoln S, Lackner LL, Glass IA, Hoppins S. Aberrant Drp1-mediated mitochondrial division presents in humans with variable outcomes. Hum Mol Genet. 2018;27:3710–9.
54. Wu T, He F, Xiao N, Han Y, Yang L, Peng J. Phenotype–genotype analysis in 135 children with mitochondrial disease. Pediatr Neurol. 2022;132:11–8.
55. Yoon G, Malam Z, Paton T, Marshall CR, Hyatt E, Ivakine Z, Scherer SW, Lee KS, Hawkins C, Cohn RD. Finding of Rare Disease Genes (FORGE) in Canada Consortium Steering Committee. Lethal disorder of mitochondrial fission caused by mutations in *DNM1L*. J Pediatr. 2016;171:313–e62.

56. Zaha K, Matsumoto H, Itoh M, Saitsu H, Kato K, Kato M, Ogata S, Murayama K, Kishita Y, Mizuno Y, Kohda M, Nishino I, Ohtake A, Okazaki Y, Matsumoto N, Nonoyama S. *DNM1L*-related encephalopathy in infancy with Leigh syndrome-like phenotype. Clin Genet. 2016;90:472–4.
57. Díaz-Rodríguez SM, Herrero-Turrión MJ, García-Peral C, Gómez-Nieto R. Delving into the significance of the His289Tyr single-nucleotide polymorphism in the glutamate ionotropic receptor kainate-1 (*Grik1*) gene of a genetically audiogenic seizure model. Front Mol Neurosci. 2024;16:1322750.
58. Capriotti E, Fariselli P, Martelli PL, Casadio R. INPS-MD: a web server to predict stability of protein variants from sequence and structure. Bioinformatics. 2016;32(16):2542–4.
59. Chen Y, Lu H, Zhang N, Zhu Z, Wang S, Li M. PremPS: predicting the impact of missense mutations on protein stability. PLoS Comput Biol. 2020;16(12):e1008543.
60. Richards S, Aziz N, Bale S, Bick D, Das S, Gastier-Foster J, Grody WW, Hegde M, Lyon E, Spector E, Voelkerding K, Rehm HL, ACMG Laboratory Quality Assurance Committee. Standards and guidelines for the interpretation of sequence variants: a joint consensus recommendation of the American College of Medical Genetics and Genomics and the Association for Molecular Pathology. Genet Med. 2015;17:405–24.
61. Johnson EC, Handel TM. Effect of hydrophobic core packing on side chain dynamics. J Biomol NMR. 1999;15(2):135–43.
62. Marabotti A, Del Prete E, Scafuri B, Facchiano A. Performance of web tools for predicting changes in protein stability caused by mutations. BMC Bioinformatics. 2021;22(Suppl 7):345.
63. Kalia R, Wang RY, Yusuf A, Thomas PV, Agard DA, Shaw JM, Frost A. Structural basis of mitochondrial receptor binding and constriction by DRP1. Nature. 2018;558(7710):401–5.
64. Kraus F, Roy K, Pucadyil TJ, Ryan MT. Function and regulation of the divisome for mitochondrial fission. Nature. 2021;590:57–66.
65. Ban-Ishihara R, Ishihara T, Sasaki N, Mihara K, Ishihara N. Dynamics of nucleoid structure regulated by mitochondrial fission contributes to cristae reformation and release of cytochrome c. Proc Natl Acad Sci U S A. 2013;110:11863–8.

Table 1

Table 1 is available in the Supplementary Files section.

Figures

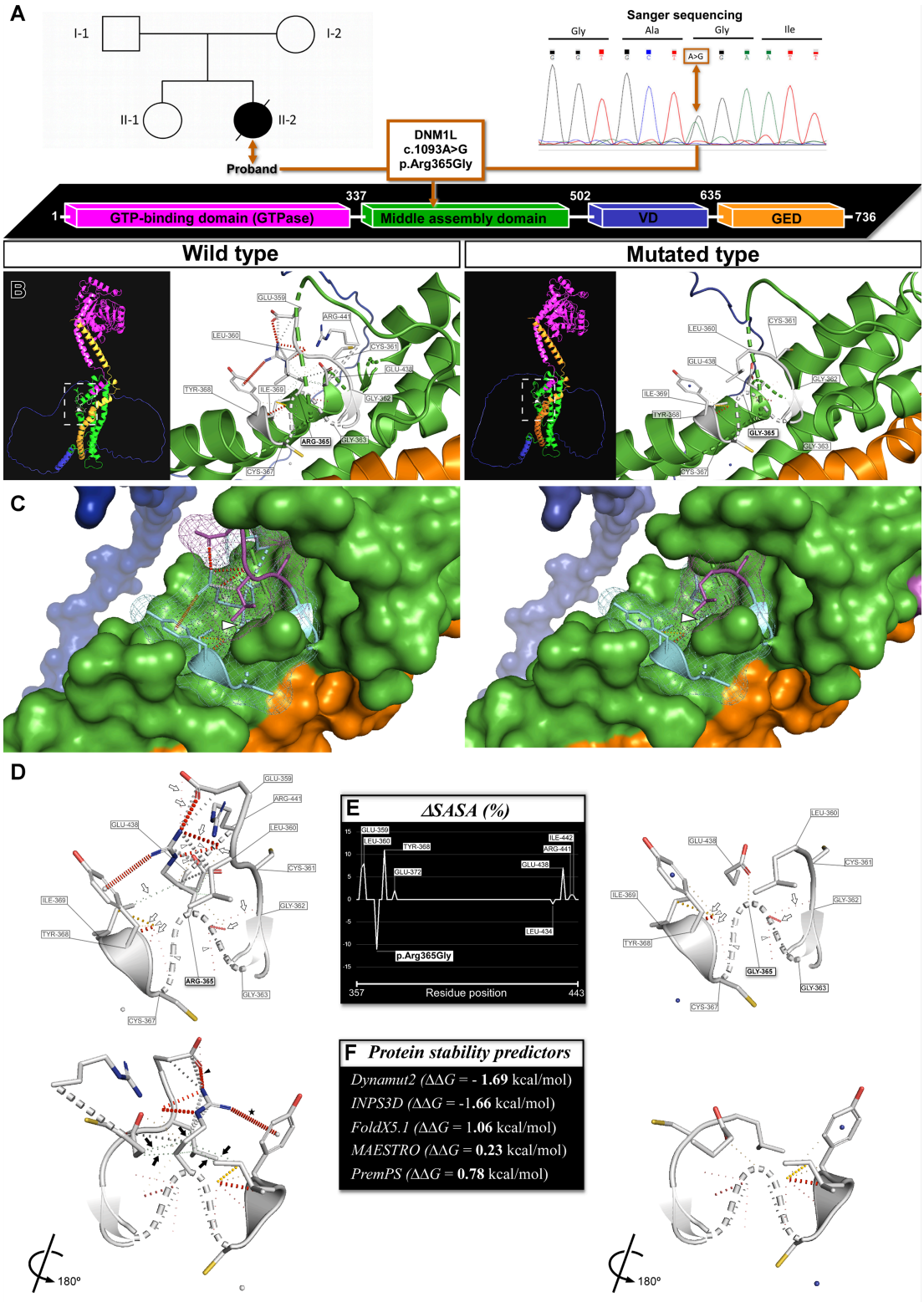


Figure 1

Identification of *de novo* p.Arg365Gly variant in *DNM1L* and structural consequences on the DRP1 protein. (A) Family pedigree showing the proband (II-2). The affected individual is shaded in black; squares denote males, circles denote females, and a diagonal line indicates a deceased individual. Sanger sequencing confirmed the heterozygous *DNM1L* variant c.1093A>G (p.Arg365Gly) in the proband. The panel below depicts the architecture of human DRP1 (736 amino acids), including its four domains:

GD, MD, VD and GED. (B) Ribbon representation of the predicted monomeric DRP1 structure, with domains color-coded as in panel A. Close-up views of the MD (green) display the wild-type Arg365 (left) and the mutant Gly365 (right). Side-chain atoms and neighboring residues are shown as sticks; molecular interactions are indicated with colored dashed lines. (C) Mesh representation and secondary-structure annotation at the mutation site. Helices are shown in light blue and loops in magenta. (D) Backbone views corresponding to panel C highlight the reduction in stabilizing interactions in the mutant. The upper panels show fewer van der Waals contacts (white arrowheads) and diminished hydrogen bonds and polar interactions (white arrows). A 180° rotation reveals complete loss of hydrophobic contacts (black arrows), ionic interactions (black arrowhead), and the aromatic cation–π interaction present in the wild-type residue (black star). (E) Solvent-accessible surface area (ΔSASA, % difference) at the mutation site. (F) Predicted change in protein fold stability (ΔΔG, kcal/mol). Although stability criteria vary among predictors, all consistently classify the p.Arg365Gly substitution as destabilizing.

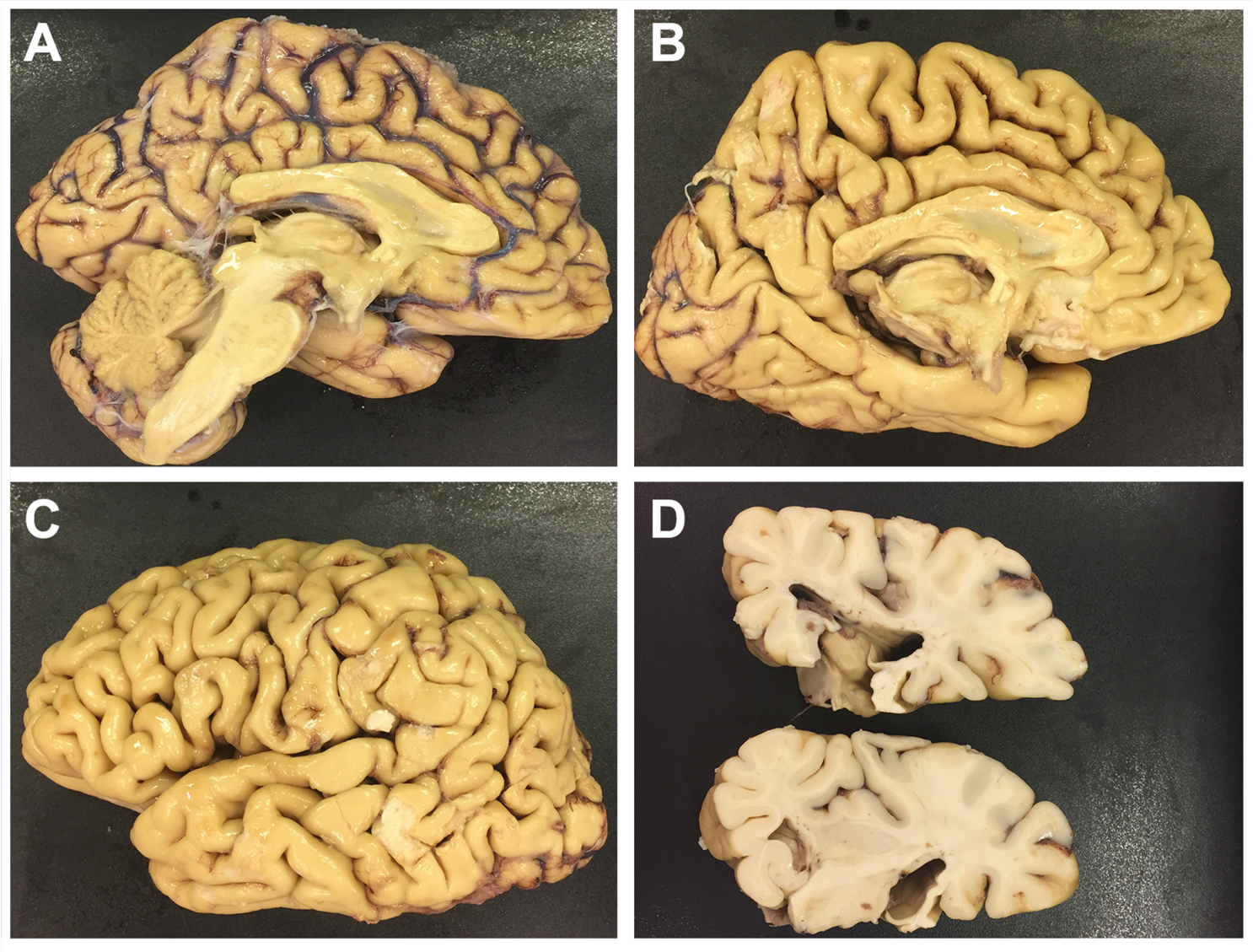


Figure 2

Macroscopic brain analysis. (A) Left hemisphere after midsagittal section. (B–C) Right hemisphere after midsagittal section. (D) Serial coronal sections of the left hemisphere showing moderate ventricular enlargement.

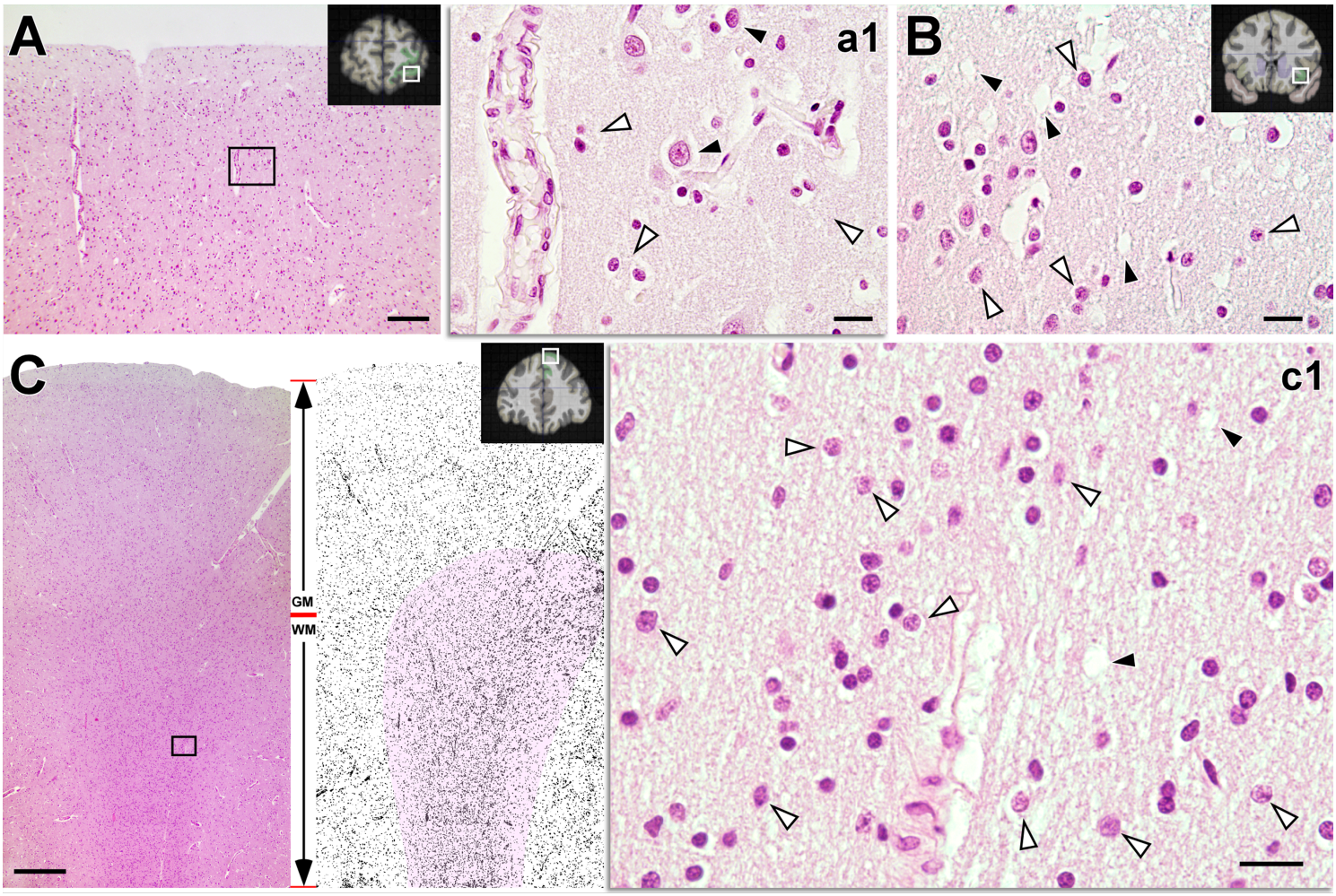


Figure 3

Histopathological alterations in the cerebral cortex and juxtacortical white matter. (A) H&E-stained section of the orbitofrontal cortex shows marked disruption of the normal laminar cytoarchitecture, with pronounced spongiosis and gliosis. (a1) Higher magnification of the boxed area in A shows fine microvacuolation of the neuropil (spongiosis, black arrowheads), shrunken neuronal somata, and numerous small, hyperchromatic glial nuclei indicative of gliosis (white arrowheads). (B) Higher magnification of the insular cortex showing similar features of spongiosis (black arrowheads) and gliosis (white arrowheads). (C) H&E-stained section and corresponding cell-dot scheme of the frontal cortex illustrating cortical delamination, spongiosis and gliosis at the cortico–subcortical boundary extending ventrally into the underlying white matter (area in magenta). (c1) Higher magnification of the boxed area in C depicting spongiform changes (black arrowheads) and reactive gliosis (white arrowheads). A schematic coronal brain section adapted from the Human Allen Brain Atlas indicates the approximate localization of the representative H&E section. Abbreviations: GM, grey matter; WM, white matter. Scale bars = 200 mm in A; 500 mm in C; 20 mm in a1, B and c1.

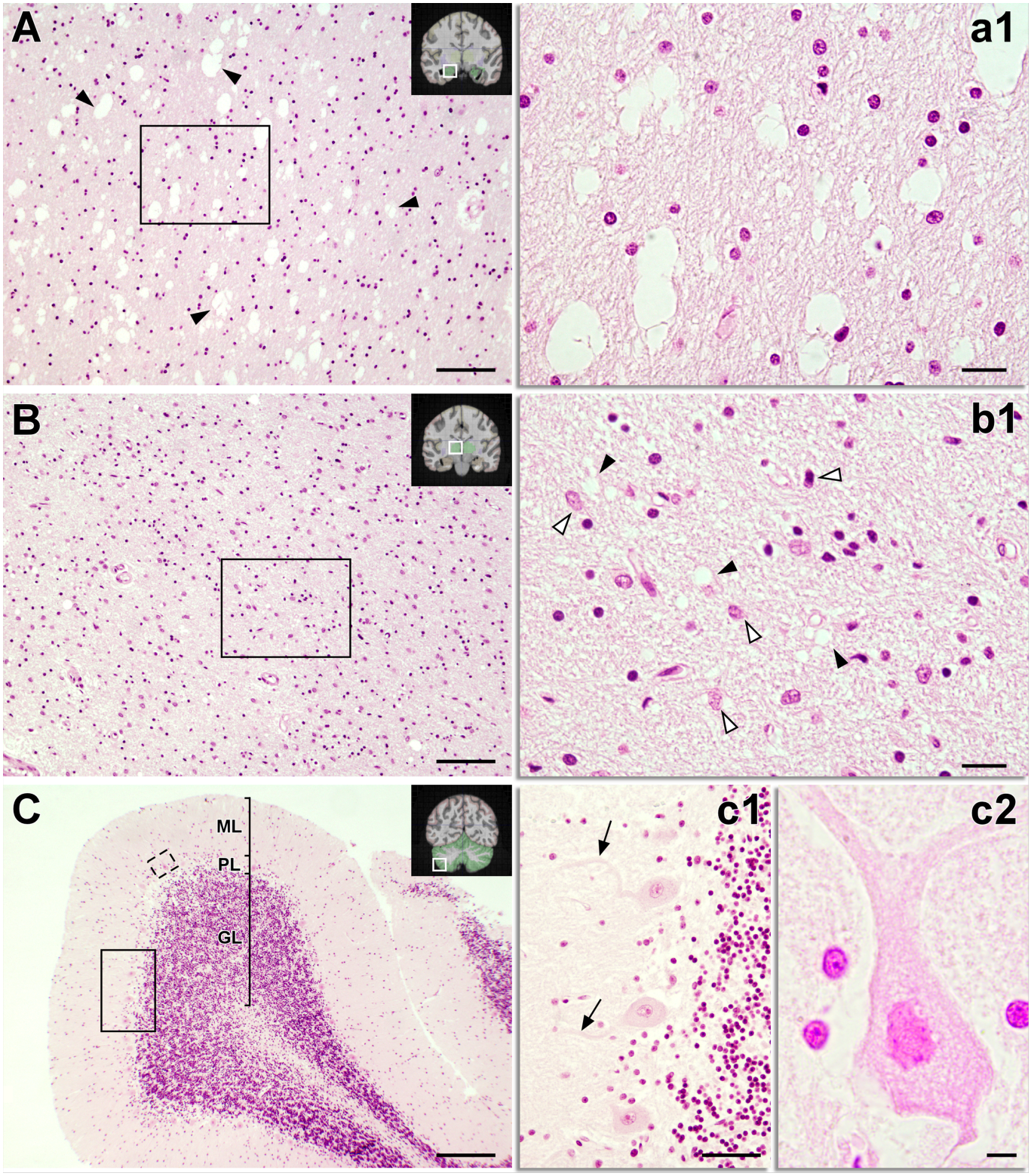


Figure 4

Histopathological alterations in the hippocampus and subcortical regions. (A) H&E-stained section of the hippocampal white matter showing moderate and widespread spongiosis (black arrowheads). (a1) Higher magnification of the boxed area in A detailing vacuolation within the neuropil. (B) H&E-stained section of the posterior hypothalamus exhibiting widespread gliosis. (b1) Higher magnification of the boxed area in B showing glial proliferation and hypertrophy (white arrowheads) accompanied by

vacuolization (black arrowheads). (C) H&E-stained section of the cerebellar cortex showing preservation of its characteristic laminar organization, composed of three distinct layers: molecular layer (ML), Purkinje cell layer (PL), and granular layer (GL). (c1-c2) Higher magnification of the boxed areas in C shows preserved Purkinje cell organization, where the pale-staining neurons exhibit dendrites extending clearly into the molecular layer (arrows) and cytoplasmic microvacuolation. A schematic coronal brain section adapted from the Human Allen Brain Atlas indicates the approximate localization of the representative H&E sections. Scale bars = 100 mm in A and B; 20 mm in a1 and b1; 200 mm in C; 50 mm in c1; 20 mm in c2.

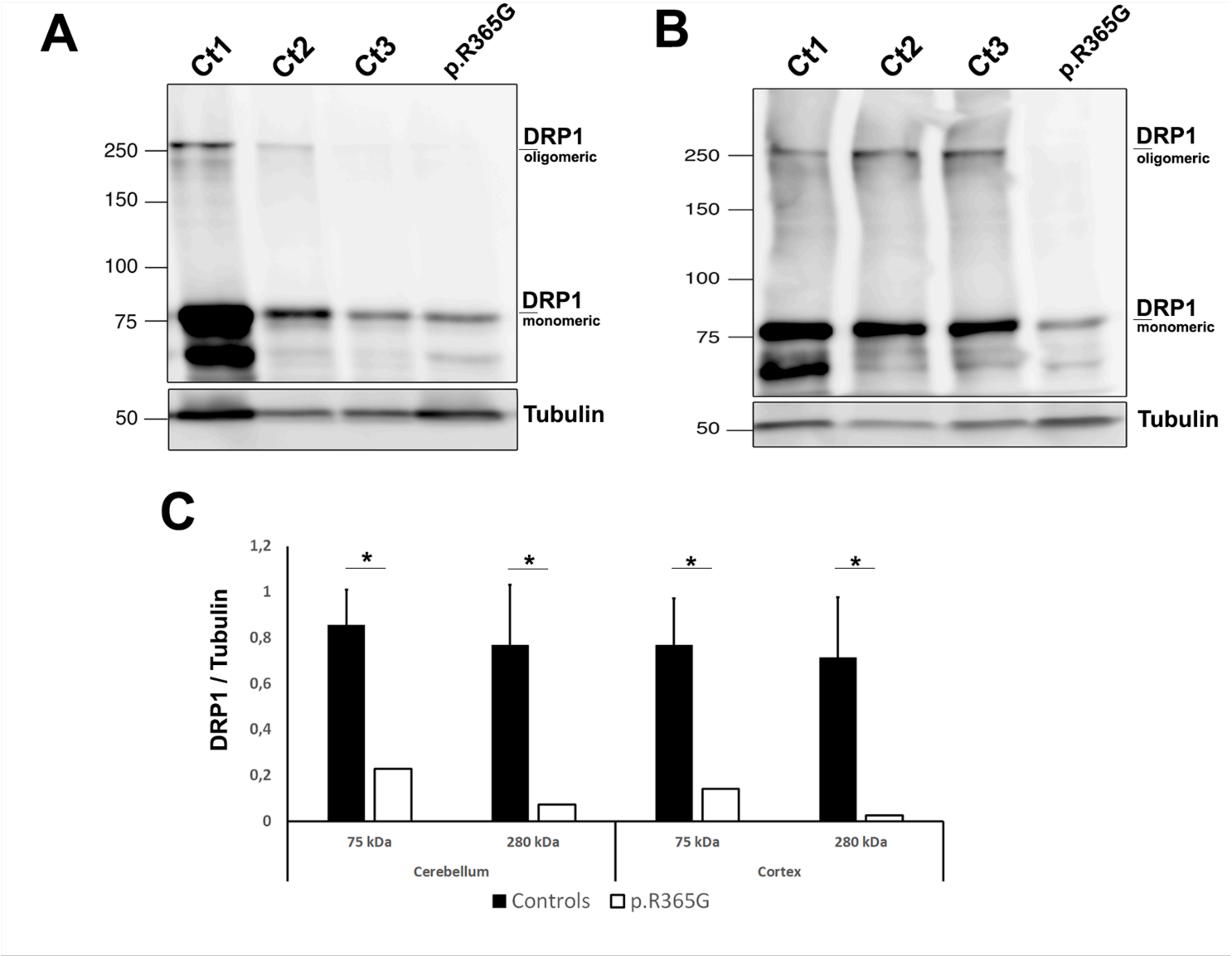


Figure 5

Western blot and quantification of DRP1 expression. Whole-cell lysates from cerebellum (A) and prefrontal cortex (B) of three controls (Ct1, Ct2 and Ct3) and the p.Arg365Gly variant, probed with DRP1 and Tubulin antibodies. Tubulin was used as a loading control. (C) Quantification of DRP1 expression levels. Data are presented as mean ± SD. *p < 0.05.

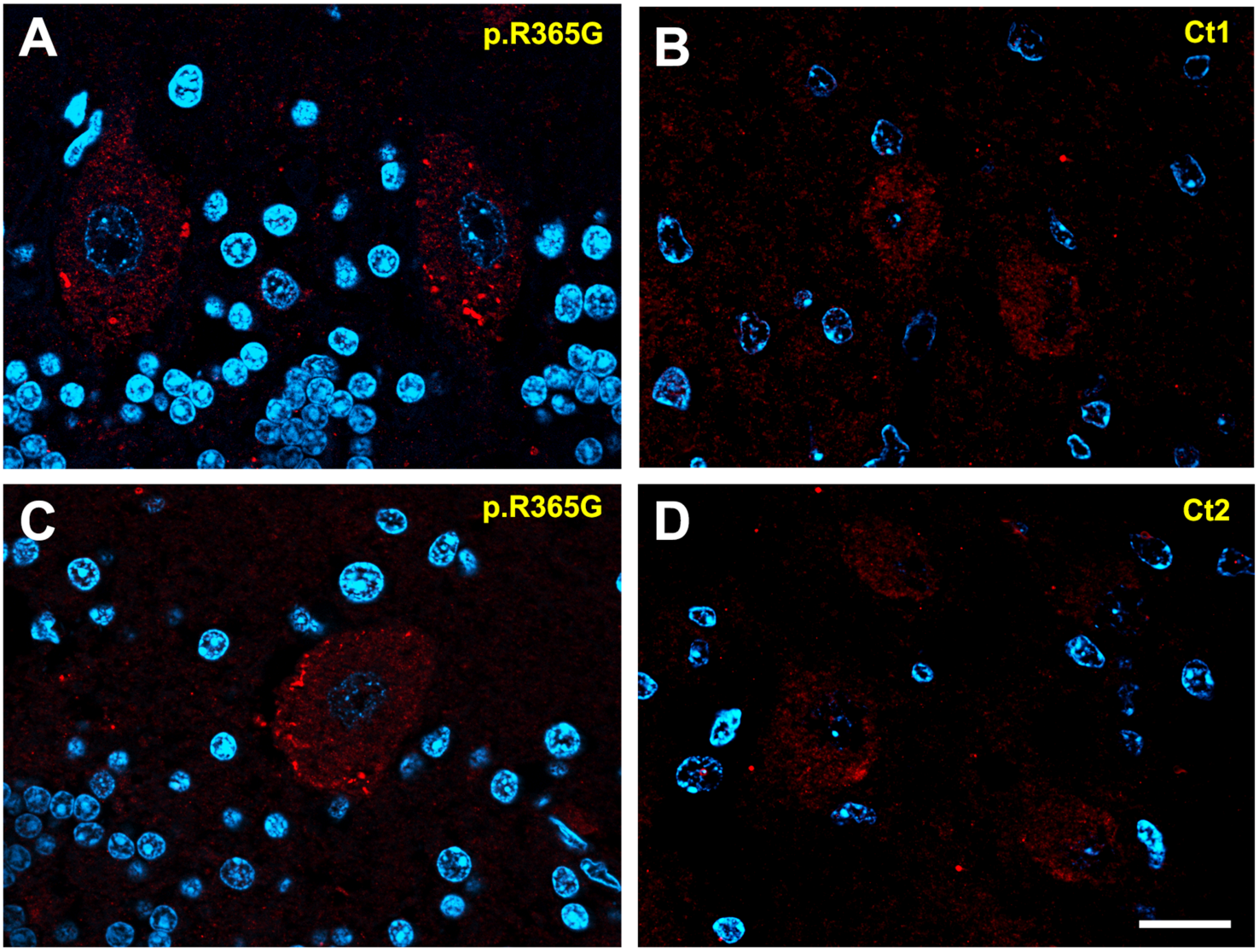


Figure 6

DRP1 immunofluorescence in cerebellar neurons. Confocal images of cerebellar neurons from the patient with the p.Arg365Gly variant compared to two pediatric controls (Ct1 and Ct2). DRP1 is shown in red. Scale bar: 10 µm.

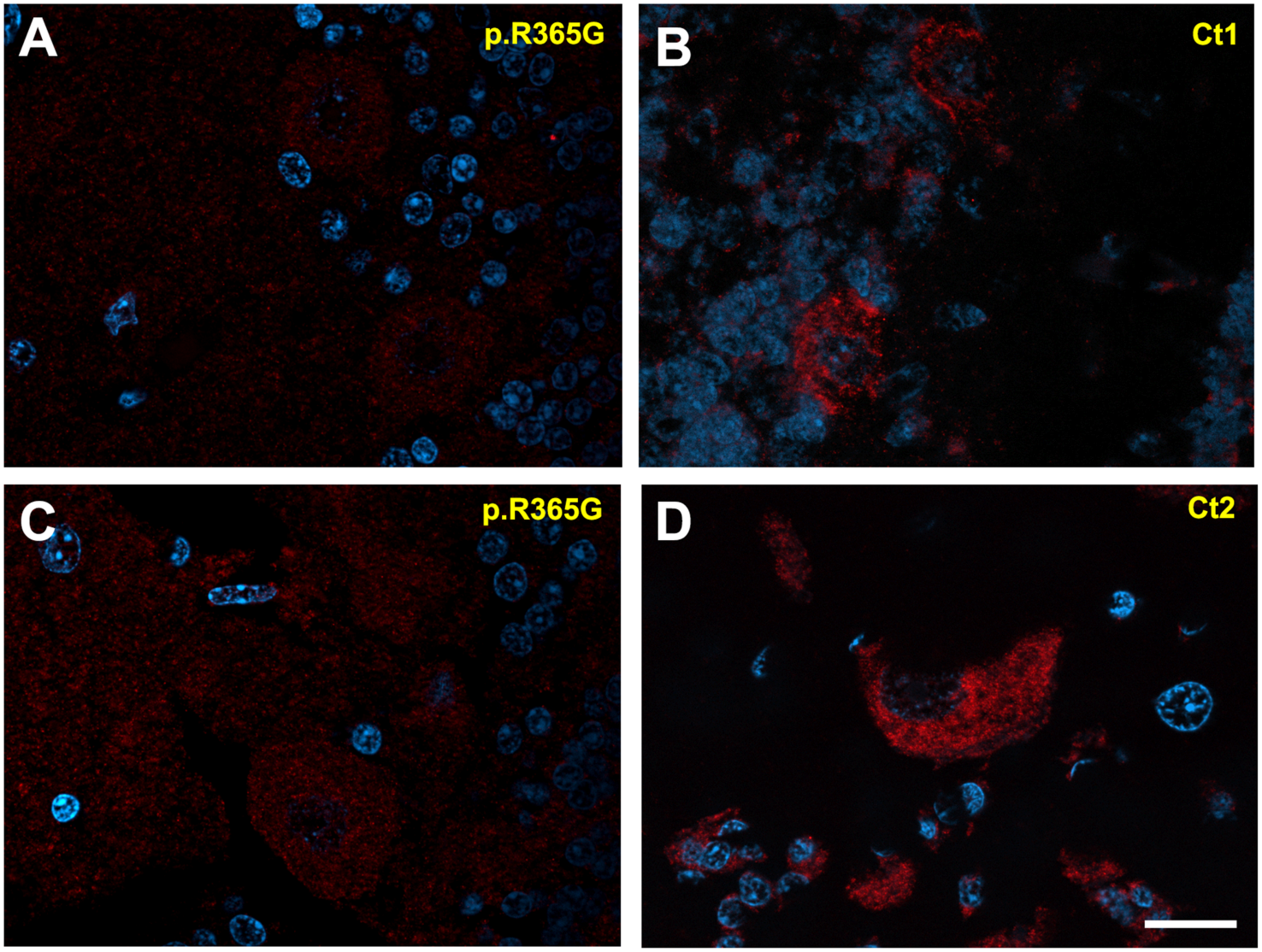


Figure 7

Mitochondrial morphology in cerebellar neurons. Confocal images of cerebellar neurons from the patient with the p.Arg365Gly variant compared to two pediatric controls (Ct1 and Ct2). Mitochondria are labeled with anti-TOMM20 (red). Scale bar: 10 µm.

Supplementary Files

This is a list of supplementary files associated with this preprint. Click to download.

- Table1.xlsx
- Supplementarymaterial1.mp4
- Supplementaryfile.rar